


Nonequilibrium Green's function approach to low-energy fission dynamics: Fluctuations in fission reactions

K. Uzawa and K. Hagino *Department of Physics, Kyoto University, Kyoto 606-8502, Japan*

(Received 7 March 2024; revised 19 June 2024; accepted 28 June 2024; published 22 July 2024)

We present a microscopic modeling for a decay of a heavy compound nucleus, starting from a nucleonic degree of freedom. To this end, we develop an approach based on a nonequilibrium Green's function, which is combined with a configuration-interaction approach based on a constrained density-functional theory. We apply this approach to a barrier-top fission of ^{236}U , restricting the model space to seniority zero configurations of neutrons and protons. We particularly focus on the distribution of the fission probability. We find that it approximately follows the χ^2 distribution with the number of degrees of freedom ν of the order of 1, which is consistent with the experimental finding. We also show that ν corresponds to the number of those eigenstates of the many-body Hamiltonian which have significant components on both sides of a fission barrier and at the same time whose eigenenergy is close to the excitation energy of the system.

DOI: [10.1103/PhysRevC.110.014321](https://doi.org/10.1103/PhysRevC.110.014321)

I. INTRODUCTION

Heavy compound nuclei decay by emitting particles such as neutrons, protons, and alpha particles, as well as via fission. It has been a custom to describe such decays of a compound nucleus using a statistical model [1,2]. While a level density is an important microscopic input to a statistical model, dynamical calculations based on a many-body Hamiltonian has been rather scarce [3].

The purpose of this paper is to develop a microscopic description of decays of a heavy compound nucleus, particularly a competition between radiative capture and fission. There are many motivations for this. Firstly, in r-process nucleosynthesis, heavy neutron-rich nuclei may decay via fission, leading to a fission recycling [4–6]. Such heavy neutron-rich nuclei are located outside the experimentally known region, and a description of fission with a microscopic framework is desirable. Secondly, a neutron separation energy of neutron-rich nuclei is so small that a compound nucleus formed in r-process nucleosynthesis will be at relatively low excitation energies. One may then question the validity of a statistical model, and thus a microscopic approach would be more suitable in that situation. This would be the case also for a barrier-top fission of stable nuclei in which the excitation energy at a saddle of fission barrier will be small due to the presence of a barrier. An advantage of our model is that a competition between (n, γ) and (n, f) processes can be described within the same framework. Thirdly, because of a rapid increase of computer powers, a large-scale calculation can now be performed much more easily than before. A microscopic description of fission has been an ultimate goal of nuclear physics, and we are now at the stage to tackle it with large-scale calculations [3].

In this paper we propose a microscopic approach to low-energy induced fission based on a configuration-interaction (CI) method. This is based on entirely microscopic nucleon

interactions except for input of empirical compound-nucleus properties and the height of the first fission barrier. For this purpose we apply a nonequilibrium Green's function (NEGF) [7] to describe decay dynamics. This approach has been widely utilized to calculate a current and a charge density for problems of electron transport in nanodevices [8,9]. A problem of fission has an analogous feature to this problem, as one has to estimate a transmission coefficient for a transition from a compound-nucleus configuration to a prefission configuration. This can be viewed as a nonequilibrium current.

A preliminary calculation with this approach has been published in Ref. [10]. In that paper, the model space was reduced by considering only neutron seniority-zero configurations in ^{236}U . Moreover, only the dynamics around the first fission barrier was discussed, while ^{236}U is known to have a double humped fission barrier. In this paper, we shall substantially enlarge the model space, including both neutrons and protons, and also both the first and the second fission barriers. Such extension of the model space allows a more consistent comparison with experimental data.

With the extended model space, we shall focus particularly on the distribution of fission width. Decay widths of a compound nucleus are known to follow the χ^2 distribution. This distribution is characterized by the degrees of freedom ν [11,12], which reflects the number of open exit channels. For example, neutron decay widths of very-low-energy neutrons on a target with spin zero are well described by the χ^2 distribution with $\nu = 1$, since there is only a single (*s*-wave) open channel [13]. There are typically many open exit channels for fission decays, reaching the order of 10^{10} for low-energy induced fission [14]. However, the observed large fluctuations in the fission decay widths require small values of the fitted ν parameter. For example, ν for the $^{235}\text{U}(n, f)$ reaction was found to be 2.3 ± 1.1 by fitting the experimental width distribution to the χ^2 function [11]. In the analysis of more recent

and precise data of the same reaction, the distributions were well fitted by the χ^2 distribution with $\nu = 2$ [15]. For different target nuclei, ^{233}U and ^{239}Pu , the degrees of freedom have the same order of magnitudes [16,17].

The small values of ν are explained by assuming that fission takes place through a few transition states above a fission barrier. Thus the number of degrees of freedom corresponds to the number of open transition states. Such transition state hypothesis was introduced in the theory of nuclear fission by Bohr and Wheeler [18]. While this has been widely applied to estimate the average fission widths, its derivation usually relies on the classical statistical mechanics. Even though there have been recent attempts with the random matrix approach [19–21], its consistency with quantum mechanics has not yet been fully clarified. In this paper we discuss the underlying mechanism of the small ν from a microscopic point of view.

The paper is organized as follows. In Sec. II we will explain the formulation of our configuration-interaction model. In Sec. III we will apply the model to the neutron-induced fission of ^{235}U and demonstrate that our model yields a small number of ν . We will also discuss its microscopic origin in terms of the behavior of eigenstates of a Hill-Wheeler equation. Finally, in Sec. IV we will summarize the paper and discuss future perspectives.

II. MODELING-INDUCED FISSION REACTIONS

A. Theoretical framework

We treat a fission process as a transition from a compound-nucleus state to a prefission state through many-particle many-hole configurations along a fission path. To this end, we first discretize the fission path and obtain the local ground state for each point based on the constrained density-functional theory (DFT) method. We then construct many-particle many-hole configurations on top of them. Based on the idea of the generator coordinate method (GCM), the total wave function is described as

$$|\Psi\rangle = \int dQ \sum_{\mu} f(Q, E_{\mu}) |Q, E_{\mu}\rangle, \quad (1)$$

where $|i\rangle \equiv |Q, E_{\mu}\rangle$ represents a Slater determinant characterized by the deformation parameter Q and the excitation energy E_{μ} from the local ground state. Notice that, unlike the usual GCM [22], the wave function includes not only the local ground states but also many-particle many-hole excited states. The GCM kernels are then defined as

$$H_{i,i'} = \langle i | \hat{H} | i' \rangle = \langle Q, E_{\mu} | \hat{H} | Q', E_{\mu'} \rangle, \quad (2)$$

$$N_{i,i'} = \langle i | i' \rangle = \langle Q, E_{\mu} | Q', E_{\mu'} \rangle. \quad (3)$$

After we construct those kernels based on the constrained DFT method, we add imaginary parts $-\frac{i}{2}\Gamma_a$ to the Hamiltonian kernel, Eq. (2), corresponding to the decay width to a channel a . Our model includes a single neutron entrance channel, multiple capture channels, and multiple fission channels denoted by Γ_{in} , Γ_{cap} , and Γ_{fis} , respectively. Here, Γ_{in} and Γ_{cap} have components in the compound-nucleus states, while Γ_{fis} has components in the prefission states.

The transmission coefficient from a channel a to a channel b is computed with the Datta formula [8],

$$T_{a,b}(E) = \text{Tr}[\Gamma_a G(E) \Gamma_b G^\dagger(E)], \quad (4)$$

where E is the excitation energy of a compound nucleus, and the nonequilibrium Green function $G(E)$ is given by

$$G(E) = \left[EN - \left(H - \frac{i}{2}(\Gamma_{\text{in}} + \Gamma_{\text{cap}} + \Gamma_{\text{fis}}) \right) \right]^{-1}. \quad (5)$$

Note that we do not need to solve the Hill-Wheeler equation if the Green function is constructed with a matrix inversion technique [23]. In our model, the input channel a corresponds to a neutron channel, while the output channel b is either a fission channel or a capture channel.

B. Chi-squared distribution and its degrees of freedom

In this paper we will discuss a fluctuation of the transmission coefficients for the fission channel, $T_{\text{in,fis}}$, and its relation to the χ^2 distribution. Here, the χ^2 distribution $P_\nu(x)$ is defined as

$$P_\nu(x) = \frac{\nu}{2\Gamma(\nu/2)} \left(\frac{\nu x}{2} \right)^{\nu/2-1} e^{-\nu x/2}. \quad (6)$$

The parameter ν is referred to as degrees of freedom, and Γ is the Gamma function. Empirically, the decay width of compound-nucleus states is known to closely follow the χ^2 distribution in many cases [11].

Note that the transmission coefficient obtained with Eq. (4) includes the fluctuations of both the input channel a and the output channel b . Therefore we use the fission probability [24],

$$P_{\text{fis}} \equiv T_{\text{in,fis}}/T_{\text{in}} \sim T_{\text{in,fis}}/(T_{\text{in,fis}} + T_{\text{in,cap}}), \quad (7)$$

rather than $T_{\text{in,fis}}$ itself. Here, the relation $T_n \simeq T_{\text{in,fis}} + T_{\text{in,cap}}$ is derived from the unitarity of the S matrix, and its validity has been confirmed in the Appendix in Ref. [10]. An advantage to use P_{fis} is that the fluctuation of the input channel is canceled out in between the denominator and the numerator.

III. APPLICATION TO $^{235}\text{U}(n, f)$

A. A setup of the model

Let us now apply the theoretical framework to a neutron-induced fission reaction, $^{235}\text{U}(n, f)$. To this end, we construct the GCM basis functions, $|Q, E_{\mu}\rangle$, with the density-constrained DFT calculation, assuming that the fission path is given by the mass quadrupole moment, $Q_{20} \equiv Q_2$, with axial symmetry. As a DFT solver, we employ SkyAx [25], in which the Kohn-Sham equation is solved in the cylindrical coordinate space. As an energy functional, we use a Skyrme functional with the UNEDF1 parameter set [26], which has an effective mass close to 1 and thus is suitable to reproduce a reasonable level density of excited nuclei. Note that the reference states are Slater determinants; a pairing interaction is included later as a residual interaction between the states.

The fission path is discretized with a criterion that the overlap of the local ground states between the nearest neighbors is $\mathcal{N} \sim e^{-1}$ [10,23]. We extend the maximum value of Q up

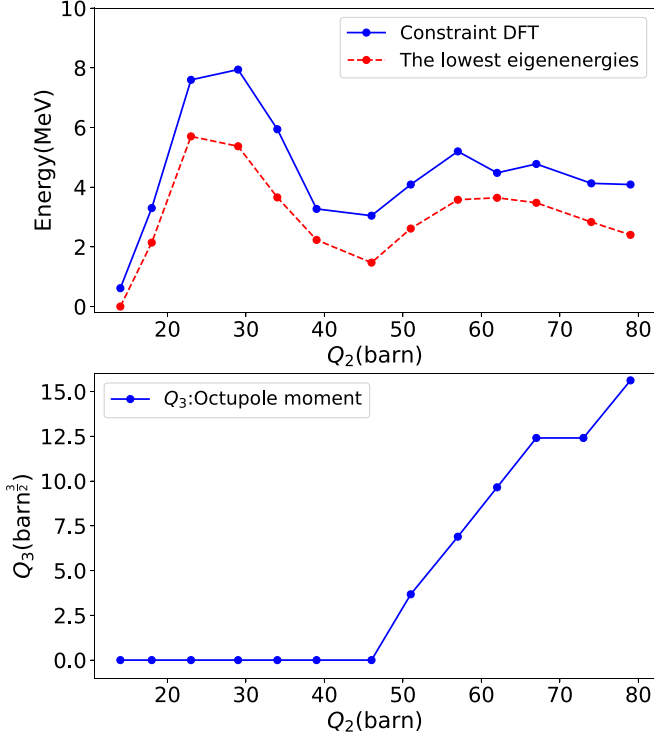


FIG. 1. (Upper panel) The fission barrier of ^{236}U along the fission path defined by the mass quadrupole moment, Q_2 . The blue solid line shows the energies of the local ground states obtained with the constrained DFT calculation. It is scaled by a factor of 0.71. The red dashed line shows the lowest eigenvalues obtained by diagonalizing each Q -block after scaling the blue solid line. The origin of the energy is set at the lowest eigenvalue at $Q_2 = 14$ b. (Lower panel) The octupole moment Q_3 in ^{236}U along the fission path.

to around 80 b so that both the first and the second fission barriers are covered. The criterion for the discretization leads to 13 blocks from $Q = 14$ b to $Q = 79$ b. The potential energy curve for fission of ^{236}U is shown in the upper panel of Fig. 1 by the blue solid line as a function of the quadrupole moment Q_2 , together with the octupole moment Q_3 shown in the lower panel. In this calculation, the ground state is located at $Q_2 = 14$ b. There are two fission barriers, the first fission barrier around $Q_2 = 30$ b and the second barrier around $Q_2 = 60$ b. The fission path is along the mass symmetric path up to the first barrier, and it extends to the mass asymmetric path going through the second barrier, as is indicated in the lower panel of Fig. 1.

In the previous work [10], the many-body configurations were constructed solely with neutron excitations up to 4 MeV. In contrast, in this paper we extend the model space and take both neutron and proton excitations up to 5 MeV. Following

Ref. [10], we shall take into account only seniority-zero configurations, that is, those without broken pairs. As a result, the dimension of the Hamiltonian kernel becomes the order of 6×10^4 . We call a sub-block in the Hamiltonian kernel for each Q a Q -block, and the dimension of each Q -block is summarized in Table I.

In the calculation of the Hamiltonian kernel, the residual interactions between configurations includes a monopole pairing component,

$$H_{\text{pair}} = -G \sum_{i \neq j} a_i^\dagger a_i^\dagger a_j a_j, \quad (8)$$

and a diabatic component [27],

$$\frac{\langle Q, E_\mu | v_{db} | Q', E_{\mu'} \rangle}{\langle Q, E_\mu | Q', E_{\mu'} \rangle} = \frac{E(Q, E_\mu) + E(Q', E_{\mu'})}{2} + h_2 \ln(\langle Q, E_\mu | Q', E_{\mu'} \rangle). \quad (9)$$

The \bar{i} in Eq. (8) denotes the time-reversal state of i . The diabatic interaction acts only between the diabatically connected configurations, $|Q, E_\mu\rangle$ and $|Q', E_{\mu'}\rangle$ [27]. We take $G = 0.16$ MeV and $h_2 = 1.5$ MeV. The value of G is determined to reproduce the excitation energy of the first excited 0^+ state of ^{236}U within the model space so specified [10], and the value of h_2 is the same as the one used in Ref. [10].

The red dashed line in the upper panel of Fig. 1 shows the potential energy curve connecting the lowest eigenvalue for each Q -block. To reproduce the experimentally determined barrier height of 5.7 MeV [28], we have introduced a multiplicative factor of 0.71 to the solid line and then diagonalized the Hamiltonian for each Q -block. At least for the first barrier, the overestimation of the barrier height may be partly attributed to the absence of the triaxial deformation [29]. We have confirmed that the results shown below remained qualitatively the same even if the rescaling was applied only to the first barrier.

As the dimension is still large for the Q -block at $Q_2 = 14$ b as well as the Q -block right after $Q_2 = 79$ b, we follow the previous calculation [10] and replace those with random matrices sampled from the Gaussian orthogonal ensemble (GOE). We set the central energy of the matrices to be the same as the excitation energy, E . In addition to the central energy, the GOE is characterized by the rms of the matrix elements $\langle v^2 \rangle^{1/2}$ and the matrix dimension N_{GOE} . These parameters are related with the level density at the center of the distribution, $\rho_0 = N_{\text{GOE}}^{1/2} / \pi \langle v^2 \rangle^{1/2}$ [30]. In our calculations, we set $\rho_0 = 31.8 \text{ MeV}^{-1}$ [10] and $N_{\text{GOE}} = 1000$. Notice that the configurations are strongly mixed after the diagonalization the GOE matrix. Therefore, a neutron can be emitted from any configuration within the GOE space, even if a single neutron

TABLE I. The dimension of each Q -block for fission of ^{236}U .

Q_2 (barn)	14	18	23	29	34	39	46	51	57	62	67	74	79	83
Dimension	N_{GOE}	2520	9794	15088	11577	2774	2940	3021	3150	2196	3752	2871	4420	N_{GOE}

channel is considered in Γ_{in} . See Appendix A for general properties of a GOE Hamiltonian, including decay widths.

The leftmost GOE matrix represents the compound-nucleus states having decay probabilities corresponding to neutron emission and γ decay. Therefore we add imaginary matrices $-\frac{i}{2}\Gamma_{\text{in}}$ and $-\frac{i}{2}\Gamma_{\text{cap}}$ to the Hamiltonian kernel. The matrix Γ_{in} has the value γ_{in} in the first diagonal component and all the other elements are zero, while Γ_{cap} has the following structure,

$$\Gamma_{\text{cap}} = \begin{pmatrix} \tilde{\Gamma}_{\text{cap}} & 0 & & \\ 0 & 0 & & \\ & & \ddots & \\ & & & 0 \end{pmatrix}, \quad (10)$$

where $\tilde{\Gamma}_{\text{cap}} = \gamma_{\text{cap}}I$, with I being the unit matrix with the dimension N_{GOE} .

Following the Appendix in Ref. [10], we set $\gamma_{\text{in}} = 0.01$ MeV and $\gamma_{\text{cap}} = 0.00125$ MeV, respectively. Those width parameters are chosen with the help of compound-nucleus phenomenology through the formula relating the transmission coefficient into the compound nucleus and the average widths of compound-nucleus states,

$$T_k = 2\pi \langle \gamma \rangle \rho. \quad (11)$$

The rightmost GOE matrix represents preffission configurations. We therefore add to it an imaginary decay matrix $-\frac{i}{2}\Gamma_{\text{fis}}$ for a fission decay. The structure of Γ_{fis} is given by

$$\Gamma_{\text{fis}} = \begin{pmatrix} 0 & & & \\ & \ddots & & \\ & & 0 & 0 \\ & & 0 & \tilde{\Gamma}_{\text{fis}} \end{pmatrix}, \quad (12)$$

where $\tilde{\Gamma}_{\text{fis}} = \gamma_{\text{fis}}I$. It has been found that transmission coefficients are insensitive to the value of γ_{fis} [10,31], and we set γ_{fis} arbitrarily to be 0.015 MeV.

Neglecting the couplings between the next-to-nearest neighboring Q -blocks,¹ the resultant Hamiltonian matrix has the following structure:

$$H = \begin{pmatrix} \tilde{H}_{\text{GOE}}^{(L)} & (V^{(L)})^T & & & \\ V^{(L)} & H_1 & V_{1,2} & & O \\ & V_{2,1} & H_2 & V_{2,3} & \\ & & & \ddots & \\ O & & & & V_{11,12} & H_{12} & (V^{(R)})^T \\ & & & & V^{(R)} & \tilde{H}_{\text{GOE}}^{(R)} & \end{pmatrix}, \quad (13)$$

where O is the zero matrix, and $\tilde{H}_{\text{GOE}}^{(L)}$ and $\tilde{H}_{\text{GOE}}^{(R)}$ denote the GOE random matrices including decay widths. H_k represents the matrix elements for the configurations at specific Q_k .

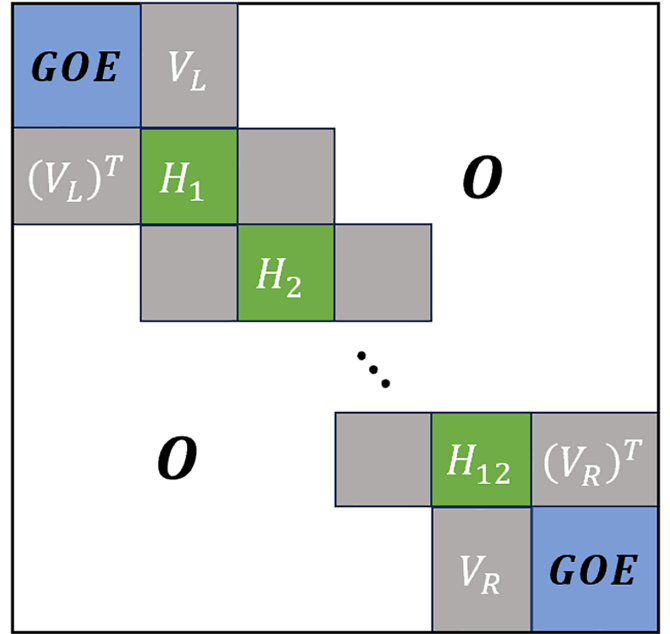


FIG. 2. A schematic illustration of the Hamiltonian matrix.

$V_{k,k'}$ denotes off-diagonal block components between neighboring configurations. We assume that the matrix elements of $V^{(L)}$ and $V^{(R)}$ also follow a Gaussian distribution, with rms strengths set to be $\sqrt{\langle v_a^2 \rangle} = 0.02$ MeV and $\sqrt{\langle v_b^2 \rangle} = 0.03$ MeV, respectively. Those orders of magnitude may be justified as follows. The present calculation with the UNEDF1 parameter set yields the level density of $\rho_{\text{tot}} = 3.87 \times 10^5 \text{ MeV}^{-1}$ for $K^\pi = 0^+$ configurations, where K is the spin projection onto the symmetry axis, at the excitation energy $E = 6.5$ MeV. On the other hand, if the configurations are restricted only to the seniority zero, the level density is $\rho_{v=0} = 220 \text{ MeV}^{-1}$ at the same excitation energy. If one scales the strength of the diabatic interaction according to the level densities, the strength of a residual interaction is estimated to be $v = h_2 \sqrt{\rho_{v=0}/\rho_{\text{tot}}} \sim 0.036$ MeV for $h_2 = 1.5$ MeV. This is close to the values of v_a and v_b which we employ.

The overlap kernel has a similar structure,

$$N = \begin{pmatrix} I^{(L)} & O & & & O \\ O & I_1 & S_{1,2} & & \\ & S_{2,1} & I_2 & S_{2,3} & \\ & & & \ddots & \\ O & & & & S_{11,12} & I_{12} & O \\ & & & & O & O & I^{(R)} \end{pmatrix}, \quad (14)$$

where I represents the identity matrix. $S_{k,k'}$ represents the overlap between neighboring Q -block configurations. As in the Hamiltonian matrix, we ignore the overlap between the next-to-nearest neighboring configurations. With this simplification, the matrix $(EN - H)$ becomes block tridiagonal, and the inversion matrix $G(E)$ can be efficiently calculated with the method presented in Ref. [32]. See Fig. 2 for a schematic illustration of the Hamiltonian matrix.

¹This approximation has been analyzed in Ref. [23].

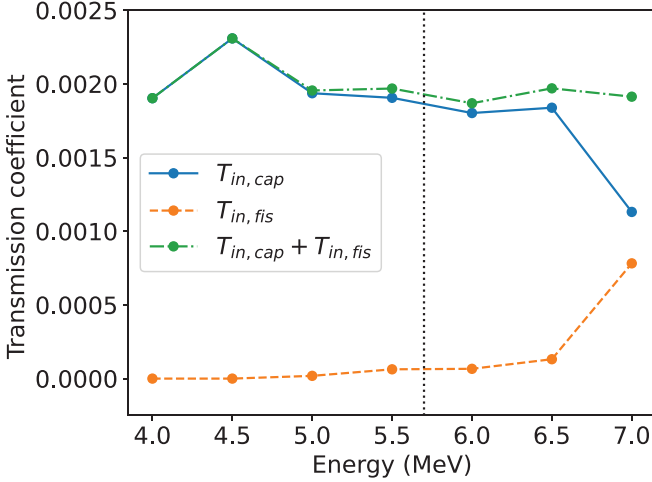


FIG. 3. The averaged transmission coefficients for capture ($\langle T_{in,cap}(E) \rangle$) (the blue solid line) and for fission ($\langle T_{in,fis}(E) \rangle$) (the orange dashed line) as a function of the excitation energy E . The sum of these transmission coefficients is also plotted with the green dot-dashed line. The vertical dotted line shows the height of the fission barrier located at 5.7 MeV.

B. The transmission coefficients

Let us now numerically evaluate the transmission coefficients, $T_{in,cap}$ and $T_{in,fis}$. Experimentally, decay widths are measured within an energy resolution. We thus introduce an energy average,

$$\langle T_{in,a}(E) \rangle = \frac{1}{\Delta E} \int_{E-\Delta E/2}^{E+\Delta E/2} dE' T_{in,a}(E'), \quad (15)$$

where ΔE is an energy interval. We take $\Delta E = 0.25$ MeV, which satisfies the condition $\Delta E \gg 1/\rho_0$. Furthermore, we take an ensemble average with 100 samples of the transmission coefficients. Figure 3 shows the energy dependence of the transmission coefficients so obtained for the capture (the solid line) and the fission (the dashed line). $\langle T_{in,fis}(E) \rangle$ increases as the excitation energy increases, while $\langle T_{in,cap}(E) \rangle$ decreases because the total reaction probability is approximately conserved (see the dot-dashed line). At $E = 6.5$ MeV, which is close to the neutron separation energy of ^{236}U ($S_n = 6.536$ MeV) [15], the fission-to-capture branching ratio, $\alpha^{-1} \equiv \langle T_{in,fis} \rangle / \langle T_{in,cap} \rangle$, is 0.071 in this calculation. Even though this value is still reasonable, it underestimates the empirical value, $\alpha^{-1} \simeq 3$ [33], by a factor of about 40. One could increase the values of ν_a and ν_b to obtain a more reasonable branching ratio. However, we have found that the fluctuation of $T_{in,fis}(E)$ then largely deviates from the χ^2 distribution, which is inconsistent with experimental findings. Since we employ the justifiable values of ν_a and ν_b , this clearly indicates that one needs to further increase the model space to reproduce the empirical branching ratio. In fact, it would be expected that the agreement with the experimental branching ratio is improved by including seniority nonzero configurations and a proton-neutron random interaction which acts on that space [31,34].

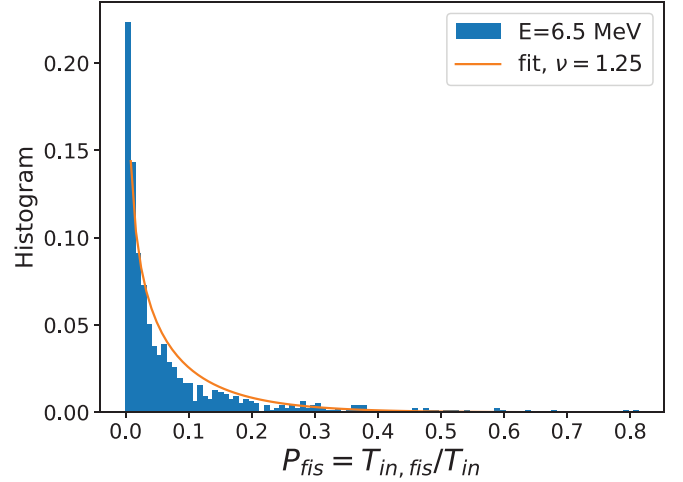


FIG. 4. Distributions of $P_{fis}(E)$ for 1000 samples at $E = 6.5$ MeV. The orange solid line shows a χ^2 distribution, with ν determined by the maximum likelihood fit. The value of ν is shown in the inset.

C. Distribution of P_{fis}

An important quantity for induced fission is the number of degree of freedom, which is related to the effective number of decay channels. In order to study this, we examine the fluctuation of the fission channel P_{fis} in Eq. (7). To this end we fit the distribution of P_{fis} generated with 1000 samples for a specific excitation energy E with the χ^2 function defined by Eq. (6). The distribution of P_{fis} at $E = 6.5$ MeV is shown in Fig. 4, while extracted values of ν are shown in Fig. 5. It is remarkable that the extracted ν is much smaller than the number of fission channels, that is, $N_{GOE} = 1000$ in this calculation. This is consistent with the picture of transition

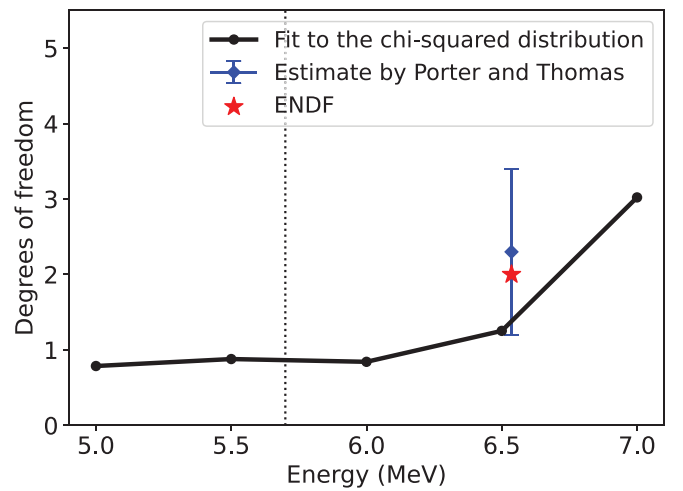


FIG. 5. The number of degrees of the freedom ν obtained by fitting the distribution of transmission coefficients for fission to the χ^2 distribution. The blue diamond is the empirical estimate of ν in Ref. [11], while the star represents the data from ENDF/B-VIII.0 [35,36]. The vertical dotted line denotes the height of the fission barrier.

state theory [18,37–43], and our model yields it naturally even though we do not introduce *a priori* any assumption used in it [44]. The value near $E = 6.5$ MeV, $\nu = 1.25$, is close to the original estimate of Porter and Thomas [11], ($\nu = 2.3 \pm 1.1$ at $E=6.536$ MeV), as well as a recent estimate based on evaluated cross-section data [35], even though the calculation somewhat underestimates the empirical values.²

Incidentally, the result shown in Fig. 5 is consistent with Fig. 3 in Ref. [45], in which the degrees of freedom ν were extracted based on the rank of Γ_{eff} defined by Eq. (17) below. The consistency of the results obtained with the different approaches strongly supports the validity of our finding of small ν .

One can see in Fig. 4 that the distribution of P_{fis} approximately follows the χ^2 distribution; however, the agreement is not perfect. We will discuss a possible origin for the deviation in the next subsection based on the effective Hamiltonian approach.

D. Effective Hamiltonian for a compound-nucleus configuration

The fact that the fission probability behaves closely to the χ^2 distribution originates from the properties of the GOE matrix (see Appendix A). To discuss how it arises, we here construct an effective Hamiltonian for the compound-nucleus configurations by eliminating the other space. As we would like to discuss the fluctuation of the fission width, in this subsection we set $\Gamma_{\text{in}} = \Gamma_{\text{cap}} = 0$ and consider the width matrix only for the fission channel. Let us write the Hamiltonian, Eq. (13), as

$$H = \begin{pmatrix} H_{\text{GOE}}^{(L)} & (\mathbf{V}^{(L)})^T \\ \mathbf{V}^{(L)} & H_Q \end{pmatrix}, \quad (16)$$

where $\mathbf{V}^{(L)}$ is defined as $\mathbf{V}^{(L)} = (V^{(L)}, O, O, \dots, O)^T$. We define N_Q in a similar way for the overlap kernel, N . The effective Hamiltonian for the space of $H_{\text{GOE}}^{(L)}$ can then be constructed as

$$\begin{aligned} H_{\text{eff}}(E) &= H_{\text{GOE}}^{(L)} - \mathbf{V}^{(L)}(H_Q - EN_Q)^{-1}(\mathbf{V}^{(L)})^T \\ &\equiv H_{\text{GOE}}^{(L)} + \Delta(E) - i\Gamma_{\text{eff}}(E)/2, \end{aligned} \quad (17)$$

where $H_{\text{GOE}}^{(L)} + \Delta(E)$ and $-\Gamma_{\text{eff}}(E)/2$ are the real and the imaginary parts of the effective Hamiltonian, respectively. $\Delta(E)$ serves as an energy shift, and $\Gamma_{\text{eff}}(E)$ corresponds to the fission width for the compound states. Notice that the width matrices, Γ_{cap} , Γ_{fis} , and Γ_{in} , have the same diagonal structure to Eq. (A1), but this may not be the case in $\Gamma_{\text{eff}}(E)$.

If $\Delta(E)$ was zero, the real part of H_{eff} became a GOE matrix itself, and the degrees of freedom of the exit channel were estimated by [46]

$$\nu = \frac{\text{Tr}[\Gamma_{\text{eff}}]^2}{\text{Tr}[(\Gamma_{\text{eff}})^2]}. \quad (18)$$

If we apply this formula to our calculation, we obtain $\nu = 1.00$ at $E = 6.5$ MeV, which is consistent with the result

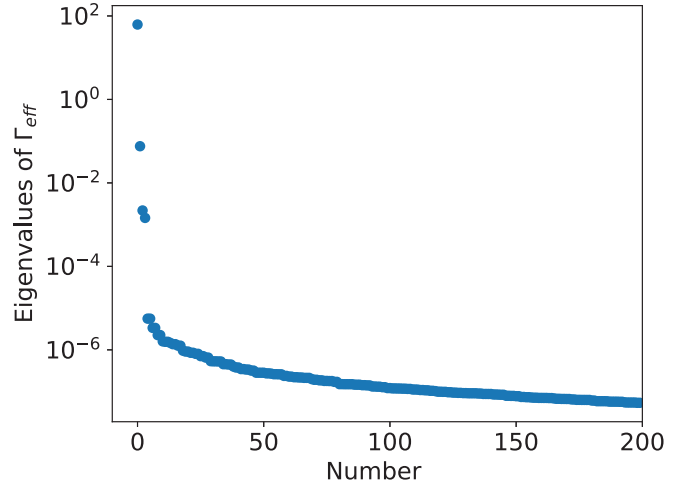


FIG. 6. Eigenvalues of the matrix Γ_{eff} at $E = 6.5$ MeV defined by Eq. (17) for a typical sample. The dimension of Γ_{eff} is 1000, and the first 200 eigenvalues are plotted in descending order.

shown in Fig. 5. The eigenvalues of Γ_{eff} at $E = 6.5$ MeV are plotted in Fig. 6 for a specific random seed. In our model, the dimension of Γ_{eff} is $N_{\text{GOE}} = 1000$, and there are 1000 eigenvalues for each ensemble. One can notice that there exists only one large eigenvalue, and the remainders are negligibly small as compared to it. Naturally, the value of ν becomes close to 1 if Eq. (18) is applied. We have confirmed that this is the case for all the samples which we study in this paper (see Appendix C).

In reality, a finite $\Delta(E)$ makes the real part of H_{eff} deviate from a pure GOE matrix, and the distribution is also perturbed from a pure χ^2 distribution. In our setup, the effect of $\Delta(E)$ is small and the distribution still follows approximately a χ^2 distribution (see Fig. 4).

E. Discussion

In the previous subsection, we have investigated the eigenvalues of the decay matrix, Γ_{eff} , and demonstrated that a fission width has small degrees of freedom. In order to understand it microscopically, let us go back to the Datta formula, Eq. (4). With the setup of our model for Γ_{in} and Γ_{fis} , this formula reads

$$T_{\text{in,fis}} = \gamma_{\text{in}}\gamma_{\text{fis}} \sum_{j \in \text{fis}} |G_{1,j}|^2. \quad (19)$$

Here the neutron channel $n = 1$ represents a specific configuration in the left-end GOE, and the fission channel includes all configurations in the right-end GOE. We then perform a spectrum decomposition of $G(E)$ as³

$$G_{ij}(E) = \sum_{\lambda} f_i^{(\lambda)} \frac{1}{E - \tilde{E}_{\lambda}} (f_j^{(\lambda)})^*, \quad (20)$$

²We expect that the agreement is improved if seniority nonzero configurations are taken into account in the model space.

³This is in contrast to the Appendix of Ref. [11], in which a decaying wave function was decomposed into transition states.

TABLE II. The breakdown of Eq. (24) at $E = 5.5$ MeV for specific eigenstates, including the dominant eigenmode (at $E_\lambda = 5.4999$ MeV) shown in the bottom panel in Fig. 7. The table also lists the value of Γ_λ defined by Eq. (22).

E_λ (MeV)	$ f_\lambda(Q_L, E_n) ^2$	$\frac{1}{(E-E_\lambda)^2+(\Gamma_\lambda/2)^2}$	$\sum_\mu f_\lambda(Q_R, E_\mu) ^2$	The product	Γ_λ (MeV)
5.4946	2.56×10^{-9}	3.51×10^4	2.82×10^{-2}	2.58×10^{-6}	4.23×10^{-4}
5.4969	1.30×10^{-5}	9.04×10^4	2.26×10^{-6}	2.68×10^{-6}	5.68×10^{-4}
5.4999	1.17×10^{-7}	6.22×10^6	5.34×10^{-2}	3.89×10^{-2}	8.02×10^{-4}
5.5008	9.54×10^{-9}	1.66×10^6	3.59×10^{-3}	5.68×10^{-5}	5.39×10^{-5}
5.5032	1.41×10^{-7}	6.57×10^4	2.96×10^{-1}	2.74×10^{-3}	4.45×10^{-3}

where $f_\mu^{(\lambda)}$ is a solution of the generalized eigenvalue problem with the GCM kernels in Eqs. (2) and (3), satisfying

$$\sum_j (H - E_\lambda N)_{ij} f_j^{(\lambda)} = 0. \quad (21)$$

Notice that $f_j^{(\lambda)}$ with $j = (Q, E_\mu)$ is equivalent to the GCM weight function $f_\lambda(Q, E_\mu)$ defined by Eq. (1). \tilde{E}_λ in Eq. (20) is defined as $\tilde{E}_\lambda = E_\lambda - \frac{1}{2}\Gamma_\lambda$, where Γ_λ is given by

$$\Gamma_\lambda = \sum_{i,j} (f_i^{(\lambda)})^* (\Gamma_{\text{in}} + \Gamma_{\text{cap}} + \Gamma_{\text{fis}})_{ij} f_j^{(\lambda)}. \quad (22)$$

Notice that for simplicity the decay matrices in the Green function are treated perturbatively. Substituting Eq. (20) into Eq. (19), we obtain

$$\begin{aligned} T_{\text{in,fis}} = & \gamma_{\text{in}} \gamma_{\text{fis}} \sum_\lambda \frac{|f_1^{(\lambda)}|^2}{(E - E_\lambda)^2 + (\Gamma_\lambda/2)^2} \sum_{j \in \text{fis}} |f_j^{(\lambda)}|^2 \\ & + \gamma_{\text{in}} \gamma_{\text{fis}} \sum_{\lambda \neq \lambda'} \sum_{j \in \text{fis}} \frac{f_1^{(\lambda)} f_1^{(\lambda')*} f_j^{(\lambda)} f_j^{(\lambda')*}}{(E - \tilde{E}_\lambda)(E - \tilde{E}_{\lambda'}^*)}. \end{aligned} \quad (23)$$

We then take an ensemble average of $T_{\text{in,fis}}$. To this end, we notice that $f_k^{(\lambda)}$ approximately follows a Gaussian distribution, and they are uncorrelated with the eigenvalues \tilde{E}_λ [44] when k is for the neutron and the fission channels. As explained in Appendix A, amplitudes of GOE eigenstates follow in general a Gaussian distribution, and this property is expected to be conserved in our model as long as the couplings between the GOE matrices and the bridge Hamiltonian are not too strong. As we have discussed in Sec. III D, we have confirmed that this is the case for the coupling strengths which we employ, that is, $\sqrt{\langle v_a^2 \rangle} = 0.02$ MeV and $\sqrt{\langle v_b^2 \rangle} = 0.03$ MeV.

As a consequence, the second term in Eq. (23) vanishes and one can take an ensemble average separately for the three factors in the first term in Eq. (23). The ensemble-averaged transmission coefficients for fission then read

$$\begin{aligned} \langle T_{\text{in,fis}}(E) \rangle &= \gamma_{\text{in}} \gamma_{\text{fis}} \sum_\lambda \langle |f_\lambda(Q_L, E_n)|^2 \rangle \left\langle \frac{1}{(E - E_\lambda)^2 + (\Gamma_\lambda/2)^2} \right\rangle \\ &\times \left\langle \sum_\mu |f_\lambda(Q_R, E_\mu)|^2 \right\rangle, \end{aligned} \quad (24)$$

where Q_L and Q_R denote the leftmost and the rightmost configurations, respectively. In this way, $T_{\text{in,fis}}$ is decomposed into a contribution of each GCM eigenmode, λ .

In order to investigate how many eigenmodes contribute to the transmission coefficient, Fig. 7 plots the contribution of each eigenmodes for $E = 5.5$ MeV as a function of E_λ . The Breit-Wigner term acts as an energy window, and the eigenmodes λ contribute significantly to $T_{\text{in,fis}}$ only when the eigenenergy E_λ is within the range $(E - \Gamma_\lambda/2, E + \Gamma_\lambda/2)$. Table II shows the breakdown of each term in Eq. (24) for five eigenstates around the dominant eigenmode. One can see that the components both at the leftmost and the rightmost Q are relatively large for the dominant eigenmode as compared to those for the other eigenmodes. This is a necessary condition to have a large transmission coefficient, as is evident from Eq. (24).

The collective wave function for the dominant eigenstate is shown in Fig. 8. Here, the collective wave function is defined as

$$g_j^{(\lambda)} = \sum_{j'} (N^{1/2})_{jj'} f_j^{(\lambda)}, \quad (25)$$

where $N^{1/2}$ is the square root of the overlap kernel, N . In the figure the square of the collective wave function is plotted as a function of Q by summing all the configurations for each Q . One can see that this wave function has a peak in the middle of a chain of the Q -blocks, rather than at the position of the higher barrier, as would have been assumed in the transition

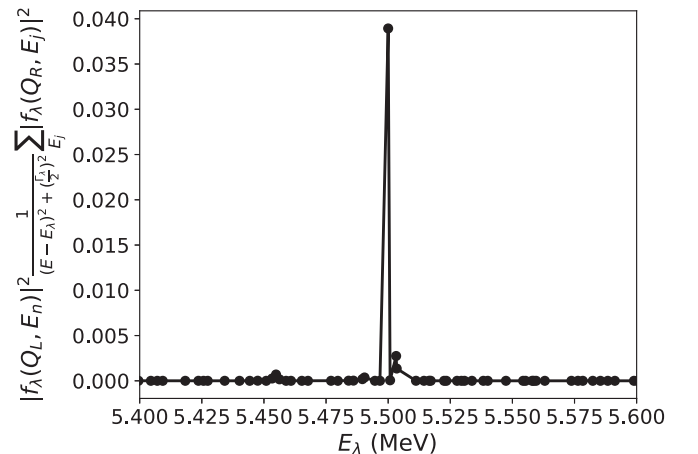


FIG. 7. The spectrum decomposition of the transmission coefficient for fission at $E = 5.5$ MeV defined by Eq. (24).

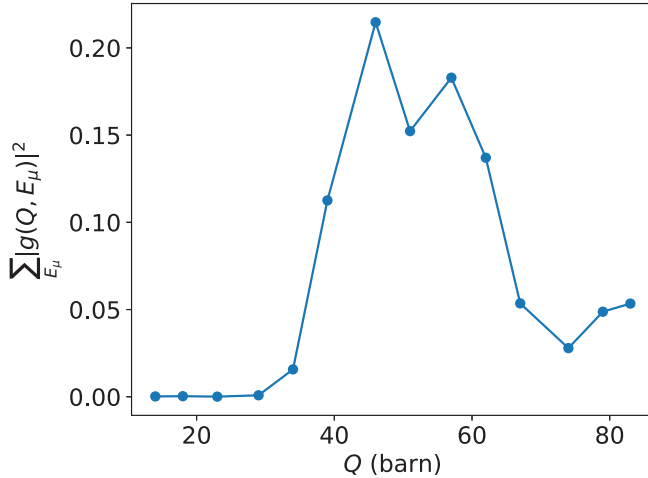


FIG. 8. The square of the collective wave function $\sum_{\mu} |g(Q, E_{\mu})|^2$ of the dominant eigenmode for the transmission coefficient for fission. This is plotted as a function of Q by adding all the excited configurations at each Q .

state theory. This can be easily understood if one uses a simple 3×3 matrix with a tridiagonal coupling,

$$H = \begin{pmatrix} e_1 & v & 0 \\ v & e_2 & v' \\ 0 & v' & e_3 \end{pmatrix}. \quad (26)$$

When the off-diagonal couplings are zero, that is, $v = v' = 0$, the three eigenvectors of this matrix read $\psi_1 = (1, 0, 0)^T$, $\psi_2 = (0, 1, 0)^T$, and $\psi_3 = (0, 0, 1)^T$. If the off-diagonal couplings are small, one can then use the first-order perturbation theory. In this weak coupling limit, only the wave function ψ_2 acquires components both in the first and the third configurations. Therefore, the eigenstate which has significant components both in the first and the third configurations has the largest component in the second configuration. A similar argument can be applied when the dimension of the matrix is larger than 3.

In this subsection we have discussed the smallness of degrees of freedom, ν , in terms of the transmission coefficient. See Appendix B and Ref. [45] for an alternative explanation of the smallness of ν based on the rank of Γ_{eff} .

IV. SUMMARY AND FUTURE PERSPECTIVES

We presented an approach to low-energy induced fission based on the method of nonequilibrium Green's function (NEGF), which has been widely used in problems of electron transport in condensed matter physics. To this end, we considered a model which consists of many-body configurations constructed with the constrained density-functional theory. Compound nucleus configurations as well as pre-fission configurations were represented by random matrices. Transmission coefficients were then evaluated with the Datta formula in the NEGF formalism. We applied this method to neutron-induced fission of ^{235}U by restricting to seniority-zero configurations. We found that the fission-to-capture branching ratio was somewhat underestimated, even though the

calculated value was still reasonable. As we chose the parameters as realistic as possible, this clearly indicated a necessity of seniority nonzero configurations. We also evaluated the number of degrees of freedom ν for fission. Our calculation yielded much smaller values for ν as compared to the number of the fission decay channels, which is consistent with the experimental data as well as the picture of transition state theory.

We have argued that the smallness of ν can be explained in terms of the number of GCM eigenstates which significantly contribute to the transmission coefficient. While the smallness of ν has been explained based on the picture of the transition state theory, in this way the smallness of ν could be explained in a natural manner without assuming *a priori* the existence of transition states.

We have found that there are three conditions for a GCM eigenstate to contribute significantly to transmission coefficients. Firstly, an eigenstate needs to have a large enough amplitude at the left-end configurations at $Q = Q_L$, at which the neutron width is defined. Secondly, it also needs to have a large enough amplitude at the right-end configurations at $Q = Q_R$, at which the fission width is defined. Lastly, the eigenenergy E_λ has to be close to the excitation energy E due to the Breit-Wigner factor in the transmission coefficient. While in the transition state theory, transition states are assumed to locate at the barrier position, GCM eigenstates that satisfy all of these three conditions do not necessarily have the dominant component at the barrier position. In fact, in our calculation with a double humped barrier, we have found that the dominant eigenmode has the largest component in between the two barriers.

The method presented in this paper provides a promising way to microscopically understand nuclear fission. A big challenge is how to manage the dimension of Hamiltonian matrix, which increases rapidly as the model space increases. In this regard, as we argued in this paper, one only needs a limited number of GCM eigenstates in order to compute transmission coefficients. One could then employ an iterative method, such as the Lanczos algorithm, to find a few eigenstates. With such a numerical technique, one could expand relatively easily the model space such that finite seniority configurations are also included. We will report on this in a separate publication [47].

As another future work, one can use the same model as the one presented in this paper to calculate a decay width for spontaneous fission and cluster decays [48–50]. It would be interesting to analyze how these decay modes are decomposed into eigenstates of the Hill-Wheeler equation.

ACKNOWLEDGMENTS

We thank G. F. Bertch for collaborations at the early stage of this work. We also thank D. A. Brown for accessing the evaluated data in Ref. [35]. This work was supported in part by JSPS KAKENHI Grants No. JP19K03861, No. JP23K03414, and No. JP23KJ1212. The numerical calculations were performed with the computer facility at the Yukawa Institute for Theoretical Physics, Kyoto University.

APPENDIX A: GAUSSIAN ORTHOGONAL ENSEMBLE AND A CHI-SQUARED DISTRIBUTION

Here we show that perturbative decay widths in the GOE follow the χ^2 distribution for ν degrees of freedom if the width matrix Γ has equal nonzero eigenvalues and rank ν , that is,

$$\Gamma = \begin{pmatrix} \gamma & & & & \\ & \ddots & & & \\ & & \gamma & & \\ & & & 0 & \\ & & & & \ddots \end{pmatrix}. \quad (\text{A1})$$

The proof is very simple. In the GOE, the amplitudes $c_i = \langle n|i \rangle$ of the basis states $|i\rangle$ in the eigenstates $|n\rangle$ follow the Gaussian distribution in the limit of a large matrix size [12]. Notice that in the first-order perturbation theory, the eigenenergy of the eigenstate $|n\rangle$ has an imaginary part of $-i\langle n|\Gamma|n\rangle/2$, where the decay width is given by

$$\langle n|\Gamma|n\rangle = \gamma \sum_{i=1}^{\nu} |c_i|^2. \quad (\text{A2})$$

This quantity is given as a summation of the squares of Gaussian-distributed variables. By definition, its distribution is the χ^2 distribution Eq. (6) with ν degrees of freedom ν .

APPENDIX B: RANK OF THE MATRIX Γ_{eff}

In Sec. III C, we explained the small number of ν in terms of the spectrum decomposition of the Green function. On the other hand, as we showed in Fig. 6, the matrix Γ_{eff} has a low-rank structure. In this Appendix we analytically evaluate the rank of Γ_{eff} to explain the smallness of ν .

From Eq. (17), Γ_{eff} is given by

$$(\Gamma_{\text{eff}})_{i,j} = 2 \sum_{kl} V_{ik} \text{Im}[(G_Q)_{kl}] (V^T)_{lj}, \quad (\text{B1})$$

where G_Q denotes the Green function corresponding to H_Q ,

$$G_Q = (EN_Q - H_Q)^{-1}. \quad (\text{B2})$$

For simplicity of notation, we have used V for $V^{(L)}$.

Here we take the same procedure as in Sec. III C and express G_Q as

$$(G_Q)_{kl} = \sum_{\lambda} O_{k\lambda} (\tilde{G}_Q)_{\lambda} O_{\lambda l}^T. \quad (\text{B3})$$

Here, $(\tilde{G}_Q)_{\lambda}$ denotes the λ th eigenvalue of G_Q and O is defined as $O = (f_1, f_2, \dots, f_N)$, with the column vectors f_{λ} representing the GCM weight functions in Eq. (1). Then Γ_{eff} is transformed to

$$\begin{aligned} (\Gamma_{\text{eff}})_{ij} &= \sum_{\lambda, E_{\mu}, E_{\mu'}} V_{i, (Q_1, E_{\mu})} f_{\lambda}(Q_1, E_{\mu}) \\ &\times \frac{\Gamma_{\lambda}}{(E - E_{\lambda})^2 + (\frac{\Gamma_{\lambda}}{2})^2} f_{\lambda}(Q_1, E_{\mu'}) V_{j, (Q_1, E_{\mu'})}, \end{aligned} \quad (\text{B4})$$

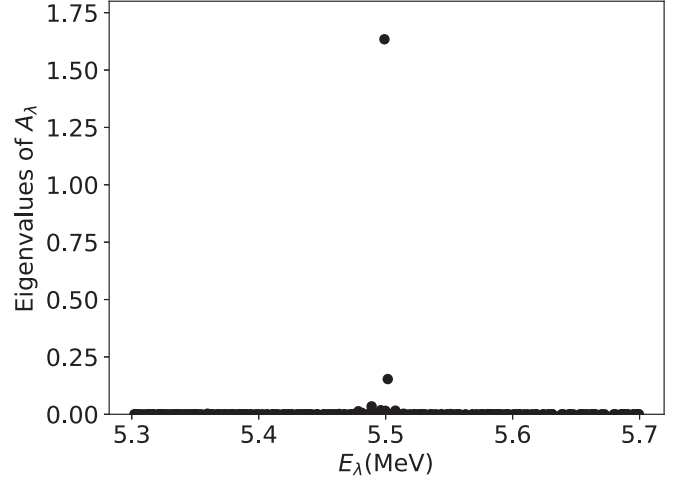


FIG. 9. Eigenvalues of A_n defined in Eq. (B5) as a function of eigenenergy E_n .

where Q_1 is the first Q -block at $Q = 18$ b, and E_{μ} denotes the label for the configurations at Q_1 . Since the rank of a matrix VAV^T is equal to the rank of the symmetric matrix A [46], the rank of the matrix Γ_{eff} is equal to the rank of $\sum_{\lambda} A_{\lambda}$, defined as

$$(A_{\lambda})_{\mu, \mu'} = f_{\lambda}(Q_1, E_{\mu}) \frac{\Gamma_{\lambda}}{(E - E_{\lambda})^2 + (\frac{\Gamma_{\lambda}}{2})^2} f_{\lambda}(Q_1, E_{\mu'}). \quad (\text{B5})$$

Using the relation

$$\text{rank}\left(\sum_{\lambda} A_{\lambda}\right) \leq \sum_{\lambda} \text{rank}(A_{\lambda}), \quad (\text{B6})$$

one can analyze the rank of each A_{λ} separately. Since the matrix A_{λ} in Eq. (B5) has a separable form, it is a rank-1 matrix. This means that A_{λ} has only one nonzero eigenvalue

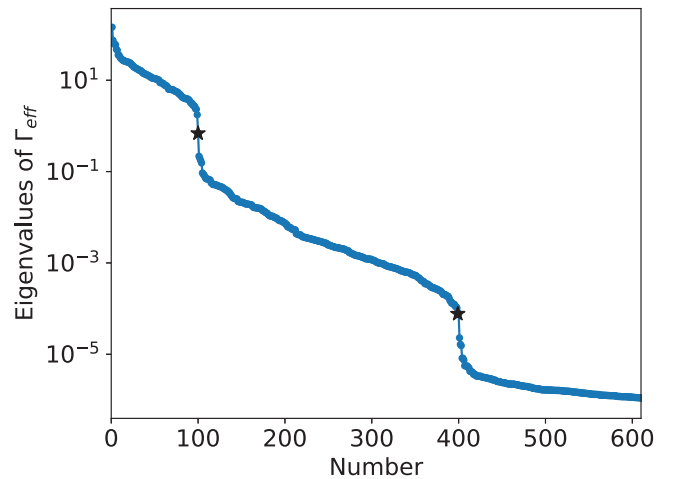


FIG. 10. Eigenvalues of Γ_{eff} at $E = 6.5$ MeV for 100 different ensembles in descending order. The 100th and 400th points are plotted by stars.

a_λ , which is equal to $\text{Tr}(A_\lambda)$. a_λ is evaluated as

$$a_\lambda = \sum_k |f_\lambda(Q_1, E_k)|^2 \frac{\Gamma_\lambda}{(E - E_\lambda)^2 + \left(\frac{\Gamma_\lambda}{2}\right)^2} \\ \simeq \left(\sum_k |f_\lambda(Q_1, E_k)|^2 \right) \frac{\gamma_{\text{fis}} \left[\sum_{E_l} |f_n(Q_R, E_l)|^2 \right]}{(E - E_\lambda)^2 + \left(\frac{\Gamma_\lambda}{2}\right)^2}. \quad (\text{B7})$$

At the last line we have evaluated Γ_λ with perturbation, see Eq. (22). This expression implies that only those eigenstates which have large enough weight at both $Q = Q_1$ and $Q = Q_R$ and whose eigenvalue E_λ is close to the excitation energy E contribute significantly to the rank of Γ_{eff} .

The eigenvalues of A_λ , that is, a_λ for our model at $E = 5.5$ MeV, are shown as a function of E_λ in Fig. 9. One can see that most of a_λ are almost zero, and only two of them have

significant values. That is, only two matrices of A_λ have rank 1, while the rest may be regarded to have rank 0. Therefore effectively $\sum_\lambda \text{rank}(A_\lambda)$ is 2, which provides the upper limit of $\text{rank}(\Gamma_{\text{eff}})$ as $\text{rank}(\Gamma_{\text{eff}}) \leq 2$. This is a direct proof why the $\text{rank}(\Gamma_{\text{eff}})$ is small, as shown in Fig. 5.

APPENDIX C: DISTRIBUTION OF EIGENVALUES OF Γ_{eff}

In Fig. 6 we plotted the distribution of the eigenvalues of Γ_{eff} for a typical sample. We have generated 100 samples and confirmed that the feature of the distribution remains the same for the different random seeds. Figure 10 shows the distribution of all those $10^3 \times 10^2 = 10^5$ eigenvalues in descending order. Reflecting the fact that there is one large and three intermediate eigenvalues in Fig. 6, the first 100 points and the subsequent 300 points form clusters. The 100th and 400th points are marked with stars in the figure.

-
- [1] P. Fröbrich and R. Lipperheide, *Theory of Nuclear Reactions* (Oxford University Press, Oxford, England, 1996).
- [2] H. Lü, A. Marchix, Y. Abe, and D. Boilley, KEWPIE2: A cascade code for the study of dynamical decay of excited nuclei, *Comput. Phys. Commun.* **200**, 381 (2016).
- [3] M. Bender *et al.*, Future of nuclear fission theory, *J. Phys. G: Nucl. Part. Phys.* **47**, 113002 (2020).
- [4] J. J. Cowan, C. Sneden, J. E. Lawler, A. Aprahamian, M. Wiescher, K. Langanke, G. Martínez-Pinedo, and F.-K. Thielemann, Origin of the heaviest elements: The rapid neutron-capture process, *Rev. Mod. Phys.* **93**, 015002 (2021).
- [5] M. Eichler, A. Arcones, A. Kelic, O. Korobkin, K. Langanke, T. Marketin, G. Martínez-Pinedo, I. Panov, T. Rauscher, S. Rosswog, C. Winteler, N. T. Zinner, and F.-K. Thielemann, The role of fission in neutron star mergers and its impact on the r-process peaks, *Astrophys. J.* **808**, 30 (2015).
- [6] S. Goriely, J.-L. Sida, J.-F. Lemaître, S. Panebianco, N. Dubray, S. Hilaire, A. Bauswein, and H.-T. Janka, New fission fragment distributions and r-process origin of the rare-earth elements, *Phys. Rev. Lett.* **111**, 242502 (2013).
- [7] S. C. K. Y. Camsari and S. Datta, *Springer Handbook of Semiconductor Devices* (Springer, Cham, Switzerland, 2023), pp. 1583–1599.
- [8] S. Datta, *Electronic Transport in Mesoscopic Systems* (Cambridge University Press, Cambridge, England, 1995).
- [9] S. Datta, *Quantum Transport: Atom to Transistor* (Cambridge University Press, Cambridge, England, 2005).
- [10] G. F. Bertsch and K. Hagino, Modeling fission dynamics at the barrier in a discrete-basis formalism, *Phys. Rev. C* **107**, 044615 (2023).
- [11] C. E. Porter and R. G. Thomas, Fluctuations of nuclear reaction widths, *Phys. Rev.* **104**, 483 (1956).
- [12] T. A. Brody, J. Flores, J. B. French, P. A. Mello, A. Pandey, and S. S. M. Wong, Random-matrix physics: Spectrum and strength fluctuations, *Rev. Mod. Phys.* **53**, 385 (1981).
- [13] H. I. Liou, H. S. Camarda, S. Wynchank, M. Slagowitz, G. Hacken, F. Rahn, and J. Rainwater, Neutron-resonance spectroscopy. VIII. The separated isotopes of erbium: Evidence for Dyson's theory concerning level spacings, *Phys. Rev. C* **5**, 974 (1972).
- [14] A. Michaudon, Distribution of neutron and fission widths, in *Statistical Properties of Nuclei: Proceedings of the International Conference on Statistical Properties of Nuclei, held at Albany, New York, August 23–27, 1971* (Springer US, Boston, MA, 1972), pp. 149–177.
- [15] L. C. Leal, H. Derrien, N. M. Larson, and R. Q. Wright, R-matrix analysis of ^{235}U neutron transmission and cross-section measurements in the 0- to 2.25-keV energy range, *Nucl. Sci. Eng.* **131**, 230 (1999).
- [16] H. Derrien, R-matrix analysis of ^{239}Pu neutron transmissions and fission cross sections in energy range from 1.0 keV to 2.5 keV, *J. Nucl. Sci. Technol.* **30**, 845 (1993).
- [17] H. Derrien, R-matrix analysis of neutron effective total cross section, fission cross section and capture cross section of ^{233}U in the energy range from thermal to 150 eV, *J. Nucl. Sci. Technol.* **31**, 379 (1994).
- [18] N. Bohr and J. A. Wheeler, The mechanism of nuclear fission, *Phys. Rev.* **56**, 426 (1939).
- [19] H. A. Weidenmüller, Random-matrix approach to transition-state theory, *Phys. Rev. E* **105**, 044143 (2022).
- [20] K. Hagino and G. F. Bertsch, Microscopic derivation of transition-state theory for complex quantum systems, *J. Phys. Soc. Jpn.* **93**, 064003 (2024).
- [21] H. A. Weidenmüller, Transition-state theory reexamined, *Phys. Rev. E* **109**, 034117 (2024).
- [22] P. Ring and P. Schuck, *The Nuclear Many-Body Problem* (Springer-Verlag, Berlin, 2000).
- [23] G. F. Bertsch and K. Hagino, Generator coordinate method for transition-state dynamics in nuclear fission, *Phys. Rev. C* **105**, 034618 (2022).
- [24] K. Hagino and G. F. Bertsch, Porter-Thomas fluctuations in complex quantum systems, *Phys. Rev. E* **104**, L052104 (2021).
- [25] P.-G. Reinhard, B. Schuettrumpf, and J. Maruhn, The axial Hartree-Fock + BCS code SkyAx, *Comput. Phys. Commun.* **258**, 107603 (2021).
- [26] M. Kortelainen, J. McDonnell, W. Nazarewicz, P.-G. Reinhard, J. Sarich, N. Schunck, M. V. Stoitsov, and S. M. Wild, Nuclear

- energy density optimization: Large deformations, *Phys. Rev. C* **85**, 024304 (2012).
- [27] K. Hagino and G. F. Bertsch, Diabatic Hamiltonian matrix elements made simple, *Phys. Rev. C* **105**, 034323 (2022).
- [28] L. Lindgren, A. Alm, and A. Sandell, Photoinduced fission of the doubly even uranium isotopes ^{234}U , ^{236}U , and ^{238}U , *Nucl. Phys. A* **298**, 43 (1978).
- [29] A. Staszczak, A. Baran, J. Dobaczewski, and W. Nazarewicz, Microscopic description of complex nuclear decay: Multimodal fission, *Phys. Rev. C* **80**, 014309 (2009).
- [30] H. A. Weidenmüller and G. E. Mitchell, Random matrices and chaos in nuclear physics: Nuclear structure, *Rev. Mod. Phys.* **81**, 539 (2009).
- [31] K. Uzawa and K. Hagino, Schematic model for induced fission in a configuration-interaction approach, *Phys. Rev. C* **108**, 024319 (2023).
- [32] D. E. Petersen, H. H. B. Sørensen, P. C. Hansen, S. Skelboe, and K. Stokbro, Block tridiagonal matrix inversion and fast transmission calculations, *J. Comput. Phys.* **227**, 3174 (2008).
- [33] M. S. Moore, J. D. Moses, G. A. Keyworth, J. W. T. Dabbs, and N. W. Hill, Spin determination of resonance structure in ($^{235}\text{U} + n$) below 25 keV, *Phys. Rev. C* **18**, 1328 (1978).
- [34] B. W. Bush, G. F. Bertsch, and B. A. Brown, Shape diffusion in the shell model, *Phys. Rev. C* **45**, 1709 (1992).
- [35] D. Brown, M. Chadwick, R. Capote *et al.*, ENDF/B-VIII.0: The 8th major release of the nuclear reaction data library with CIELO-project cross sections, new standards and thermal scattering data, *Nucl. Data Sheets* **148**, 1 (2018), Special Issue on Nuclear Reaction Data.
- [36] L. C. Leal, H. Derrien, N. M. Larson, and R. Q. Wright, R-matrix analysis of sup ^{235}U neutron transmission and cross sections in the energy range 0 to 2.25 keV, Technical Report No. ORNL/TM-13156, Oak Ridge National Laboratory, 1997, doi:10.2172/631239.
- [37] D. G. Truhlar, W. L. Hase, and J. T. Hynes, Current status of transition-state theory, *J. Phys. Chem.* **87**, 2664 (1983).
- [38] D. G. Truhlar, B. C. Garrett, and S. J. Klippenstein, Current status of transition-state theory, *J. Phys. Chem.* **100**, 12771 (1996).
- [39] G. Mills and H. Jónsson, Quantum and thermal effects in H_2 dissociative adsorption: Evaluation of free energy barriers in multidimensional quantum systems, *Phys. Rev. Lett.* **72**, 1124 (1994).
- [40] W. H. Miller, Quantum mechanical transition state theory and a new semiclassical model for reaction rate constants, *J. Chem. Phys.* **61**, 1823 (1974).
- [41] K. J. Laidler and M. C. King, The development of transition-state theory, *J. Phys. Chem.* **87**, 2657 (1983).
- [42] R. A. Marcus and O. Rice, The kinetics of the recombination of methyl radicals and iodine atoms, *J. Phys. Chem.* **55**, 894 (1951).
- [43] R. A. Marcus, Unimolecular dissociations and free radical recombination reactions, *J. Chem. Phys.* **20**, 359 (1952).
- [44] G. F. Bertsch and K. Hagino, Transition-state dynamics in complex quantum systems, *J. Phys. Soc. Jpn.* **90**, 114005 (2021).
- [45] K. Uzawa, K. Hagino, and G. F. Bertsch, Microscopic description of induced fission in a configuration interaction approach, [arXiv:2404.05500](https://arxiv.org/abs/2404.05500) [Eur. Phys. J. A (to be published)].
- [46] W. H. Miller, R. Hernandez, C. B. Moore, and W. F. Polik, A transition state theory-based statistical distribution of unimolecular decay rates with application to unimolecular decomposition of formaldehyde, *J. Chem. Phys.* **93**, 5657 (1990).
- [47] K. Uzawa and K. Hagino (unpublished).
- [48] K. Hagino and G. F. Bertsch, Microscopic model for spontaneous fission: Validity of the adiabatic approximation, *Phys. Rev. C* **101**, 064317 (2020).
- [49] K. Hagino and G. F. Bertsch, Least action and the maximum-coupling approximations in the theory of spontaneous fission, *Phys. Rev. C* **102**, 024316 (2020).
- [50] K. Uzawa, K. Hagino, and K. Yoshida, Microscopic description of cluster decays based on the generator coordinate method, *Phys. Rev. C* **105**, 034326 (2022).